The widely expressed fusion protein CTBS-GNG5 regulates cell cycle progression by stabilizing IGF2BP2

Running Title: CTBS-GNG5 regulates the cell cycle by stabilizing IGF2BP2

Liang Cheng [1,2,4,#], Jingtong Zhang[4,5,6,#], Xiaole Lu[1,2,#], Chenwei Yang[1,2,#], Fujun Qin[8], Yuhang Huang[1,2], Ming Huang[1,2,4], Junlin Lu[1,2,4], Sarah Lynch[3], Justin Elfman[3], Ruihui Xie[1,2,4], Shengmeng Peng[1,2,4], Siting Chen[1,2], Baoqing He[1,2], Haifeng Wang[7],Tianxin Lin [1,2,4], Hui Li[3,*], Jian Huang [1,2,4,*], Xu Chen [1,2,4*].

1 Department of Urology, Sun Yat-sen Memorial Hospital, Sun Yat-sen University, Guangzhou, Guangdong, P. R. China.

2 Guangdong Provincial Key Laboratory of Malignant Tumor Epigenetics and Gene Regulation, Sun Yat-sen Memorial Hospital, State Key Laboratory of Oncology in South China, Guangzhou, Guangdong, P. R. China.

3 Department of Pathology, School of Medicine, University of Virginia, Charlottesville, VA 22908, USA.

4 Guangdong Provincial Clinical Research Center for Urological Diseases, Guangzhou, Guangdong, P. R. China.

5 Department of Urology, Sun Yat-sen University Cancer Center, Sun Yat-sen University, Guangzhou, China

6 State Key Laboratory of Oncology in Southern China, Collaborative Innovation Center of Cancer Medicine, Guangzhou, China.

7 Department of Urology, The Second Affiliated Hospital of Kunming Medical University, Kunming, China.

8 State Key Laboratory of Metabolic Dysregulation & Prevention and Treatment of Esophageal Cancer, Tianjian Laboratory of Advanced Biomedical Sciences, Academy of Medical Sciences, Zhengzhou University, Zhengzhou, China

# Liang Cheng, Jingtong Zhang, Xiaole Lu and Chenwei Yang contributed equally to this work.

***Corresponding to:**

Xu Chen, Department of Urology, Sun Yat-sen Memorial Hospital, 107th Yanjiangxi Road, Guangzhou, China, E-mail: chenx457@mail.sysu.edu.cn;

Jian Huang, E-mail: huangj8@mail.sysu.edu.cn;

Hui Li, E-mail: hl9r@virginia.edu.

Abstract

Chimeric RNAs are increasingly recognized as important regulatory molecules, yet their roles in fundamental cellular processes within normal physiology remain largely unexplored. Here, we identify *CTBS-GNG5*, a ubiquitously expressed chimeric RNA, which exhibits housekeeping-gene-like expression patterns across diverse normal and malignant tissues. Furthermore, we developed a highly specific monoclonal antibody targeting the unique junction of the CTBS-GNG5 fusion protein and have confirmed its widespread protein expression across tissues of various origin. We demonstrate that the *CTBS-GNG5*-encoded fusion protein promotes cell cycle progression and proliferation both *in vitro* and *in vivo*. The fusion protein directly binds and stabilizes the m6A reader IGF2BP2, attenuating its degradation by the ubiquitin-mediated proteasome. The stabilization of IGF2BP2 enhances the mRNA stability of key cell cycle regulators, including *CDK1*, *TOP2A*, and *CDCA2*, thereby driving G1/S phase transition. Our findings unveil a paradigm-shifting role for a ubiquitous chimeric RNA as a central regulator of the cell cycle, bridging normal cellular homeostasis and oncogenic proliferation.

1. Introduction

Chimeric RNAs and their encoded proteins have long been recognized for their roles in cancer, where they serve as diagnostic markers and therapeutic targets [1]. Once thought to result exclusively from cancer-specific genomic rearrangements [2], chimeric RNAs are now known to also form in normal cells through mechanisms such as intergenic alternative splicing and transcriptional read-through [2-5]. These transcripts significantly expand the functional complexity of the transcriptome, generating novel proteins and non-coding RNAs [6, 7], yet their physiological functions remain largely unexplored.

A key unanswered question is whether chimeric RNAs exhibit housekeeping properties—ubiquitous expression across tissues and essential for fundamental cellular function [8-10]. Although certain chimeric RNAs, such as *DUS4L-BCAP29* and *CTNNBIP1-CLSTN1*, have been detected in both normal and cancerous tissues [2, 11-15], the existence and functional relevance of a widely expressed, essential chimeric RNA remains to be conclusively established. Previous studies have identified chimeric RNAs suggested to play housekeeping roles, as their expressions are generally ubiquitous and essential for cell maintenance and survival [3, 16]. The chimeric RNA *CTBS-GNG5*, a read-through transcript initially identified in B-cell lymphoma [17], has been widely detected across various normal tissues and cell lines, including lung, liver, bladder, and kidney [3, 16, 18]. However, the underlying mechanism by which CTBS-GNG5 influences cellular biological processes remains poorly understood.

A significant challenge in the field lies in the specific detection of fusion proteins, which is complicated by the coexistence of the parental proteins [19]. The development of fusion protein-targeted antibodies faces several limitations, including restricted antigen availability, insufficient specificity, and high purification complexity [20]; as a result, current detection methods frequently rely on epitopes shared with parental proteins, thereby compromising selectivity [21].

In this study, we developed a highly specific antibody targeting the CTBS-GNG5 fusion protein, which was found to be widely and abundantly expressed across the majority of normal and tumor tissues evaluated. Furthermore, the CTBS-GNG5 fusion protein

regulated cell proliferation both *in vitro* and *in vivo* by binding to and stabilizing the m6A reader, IGF2BP2. This interaction enhances the mRNA stability of key cell cycle regulators, including *CDK1*, *TOP2A*, and *CDCA2*, thereby promoting cell cycle progression. Our findings establish *CTBS-GNG5* as a ubiquitously expressed housekeeping chimeric RNA and reveal a novel regulatory axis that plays a central role in cellular homeostasis, with significant implications for both normal physiological processes and disease pathogenesis.

2. Results

2.1. Characterization of the chimeric RNA *CTBS-GNG5* and its antibody-specific targeted fusion protein

The chimeric RNA *CTBS-GNG5* was previously categorized as a ubiquitously expressed fusion transcript [3]. The identified fusion arises from the joining of *CTBS* exon 6 with *GNG5* exon 3 (Figure 1A). To validate *CTBS-GNG5* expression, we designed exon-specific primers to flank the chimeric junction. We validated the chimeric RNA by RT-PCR and Sanger sequencing in both UM-UC-3 and HEK293T cell lines (Figure 1B-C and Figure S1A). The *CTBS-GNG5* fusion transcript is categorized as a readthrough chimeric RNA, owing to the close genomic proximity of the adjacent parental genes located on the same chromosome. To verify this transcript originates from a single mRNA, we used reverse transcription (RT) with an oligo in *GNG5* exon 3, downstream of the junction site, followed by RT-PCR amplification of a fragment spanning exon 6 and intron 6 of *CTBS* (Figure S1B). Specific amplification was observed exclusively in reactions containing reverse transcriptase, establishing that the precursor RNA is transcribed from exon 6 of *CTBS* to exon 3 of *GNG5* (Figure S1C-D). To determine the landscape of tissues which express *CTBS-GNG5*, we utilized AGREP to scour RNA-Seq datasets for the *CTBS-GNG5* fusion junction sequence (Figure 1D). Our analysis revealed that *CTBS-GNG5* is widely expressed across the majority of samples in both the Genotype-Tissue Expression (GTEx) Portal (GTEx) and The Cancer Genome Atlas (TCGA) datasets, with high expression levels and frequency of detection (Figure 1E-F, Figure S2A-B, and Figure S3A). Through amino

acid sequence analysis and protein spatial structure via AlphaFold3, we determined that the chimeric RNA encodes an in-frame fusion protein whose N- and C-termini are identical to those of the parental *CTBS* and *GNG5* proteins, respectively (Figure 1G and Figure S4A).

To generate a monoclonal antibody specific to the CTBS-GNG5 fusion protein, a synthetic peptide spanning the junction sequence was selected for immunization to ensure the selective recognition of the chimeric protein by the resulting antibody. The antigenic sequence used was CEAKSISENGDMPNKENGD (Figure 1H). The antibody was used for immunoprecipitation and mass spectrometry in UM-UC-3 cells, which identified the presence of a partial amino acid sequence matching the chimeric protein (Figure 1I). A distinct band corresponding to CTBS-GNG5 was detected via the anti-CTBS-GNG5 antibody at the predicted size of 38kDa (Figure 1J). Furthermore, widespread expression of the fusion protein was confirmed via immunohistochemistry (IHC) in a variety of healthy and cancerous tissues (Figure 1K and Figure S4B-C). These results demonstrate that the generated antibody has high specificity for the CTBS-GNG5 fusion protein and that the fusion protein is expressed ubiquitously.

To evaluate the translational relevance of the *CTBS-GNG5* transcript, we investigated the subcellular localization of the corresponding fusion protein, as this characteristic is closely associated with its biological function. Western blot and immunofluorescence analyses revealed that the endogenous CTBS-GNG5 fusion protein and overexpression of Myc-tagged CTBS-GNG5 predominantly localized in the cytoplasm (Figure 1L-M). Collectively, these results indicate that the chimeric RNA *CTBS-GNG5* and its encoded fusion protein are widely expressed across various tissues and that we have developed an antibody specific for the detection of the CTBS-GNG5 fusion protein.

2.2. Knockdown of *CTBS-GNG5* inhibited the proliferation of both tumor and normal cells *in vitro.*

To investigate the impact of CTBS-GNG5 on cellular biological processes, we employed small interfering RNAs (siRNAs) specific to the chimeric RNA junction to effectively suppress *CTBS-GNG5* expression. Quantitative real-time PCR (qRT-PCR)

demonstrated significant downregulation of *CTBS-GNG5* after knockdown with two siRNAs, without detectable changes in the expression of the parental genes *CTBS* and *GNG5* (Figure S5A). Western blots confirmed a marked reduction in CTBS-GNG5 protein levels in all cell lines (Figure S5B). Subsequently, we investigated the functional role of CTBS-GNG5 through a series of experimental assays. Cell Counting Kit-8 (CCK-8) and colony formation assays revealed that knockdown of *CTBS-GNG5* significantly reduced cell viability across a broad range of cell types, including both tumor and normal cell lines derived from the bladder, prostate, lung, breast, and liver (Figure 2A-C). Furthermore, flow cytometry revealed that *CTBS-GNG5* depletion induced cell cycle arrest at the G0/G1 phase, accompanied by a concomitant decrease in the proportion of cells in S phase (Figure 2D). However, knockdown of *CTBS-GNG5* did not significantly affect apoptosis or the migratory capacity of either tumor or normal cells (Figure S6A-C). Collectively, these results indicate that *CTBS-GNG5* facilitates cell proliferation by regulating the G1/S phase transition *in vitro*.

2.3. Knockdown of *CTBS-GNG5* inhibited the proliferation of tumor cells *in vivo.*

To evaluate the impact of CTBS-GNG5 on cellular proliferation, we established stable cells via the Tet-On inducible gene expression system, where nontargeting control and *CTBS-GNG5*-targeting shRNA expression occurs after doxycycline treatment, in UM-UC-3, MDA-MB-231, and HepG2 cell lines. Subsequently, these cell lines were subcutaneously implanted into BALB/c nude mice (Figure 3A). Knockdown of *CTBS-GNG5 in vivo* significantly suppressed tumor growth, as indicated by reduced tumor weight, volume over time, and final size (Figure 3B-D). Furthermore, IHC staining revealed lower expression of Ki67, a well-established marker of proliferating cells, in tumors derived from *CTBS-GNG5*-silenced cells than in those derived from control cells (Figure 3E). Collectively, these findings demonstrate that *CTBS-GNG5* plays a critical role in promoting tumor cell proliferation *in vivo*.

2.4. The CTBS-GNG5 fusion protein stabilizes IGF2BP2 through the inhibition of ubiquitin-mediated degradation.

To elucidate the functional mechanism by which CTBS-GNG5 contributes to cell proliferation, we performed co-immunoprecipitation (co-IP) of the CTBS-GNG5 fusion protein coupled with immunoprecipitation-mass spectrometry (IP-MS) to identify interacting proteins. After CTBS-GNG5 pulldown in UM-UC-3 cells, we detected a distinct protein with an apparent molecular weight between 55-70 kDa via silver staining (Figure 4A); we identified the protein as IGF2BP2 via mass spectrometry (Figure S7A). We further validated the specific interaction between CTBS-GNG5 and IGF2BP2 by western blot and immunofluorescence (Figure 4B-C and Figure S7B). Furthermore, IGF2BP2 protein levels mirrored CTBS-GNG5 expression, decreasing in *CTBS-GNG5*-knockdown cells and increasing in *CTBS-GNG5*-overexpressing cells (Figure 4D). qRT-PCR revealed that knockdown of *CTBS-GNG5* did not significantly alter *IGF2BP2* mRNA levels (Figure S7C), suggesting that CTBS-GNG5 regulates IGF2BP2 primarily through posttranslational mechanisms. We therefore investigated whether the CTBS-GNG5-induced downregulation of IGF2BP2 that we observed occurred in a ubiquitin-proteasome-dependent manner. Treatment with MG132, a proteasome inhibitor, attenuated the reduction in IGF2BP2 protein levels (Figure 4E), indicating that CTBS-GNG5 mediates IGF2BP2 degradation through ubiquitination. To further validate this mechanism, we conducted ubiquitination assays in UM-UC-3, A549, and HEK293T cells. These experiments revealed that knockdown of *CTBS-GNG5* significantly increased the polyubiquitination of FLAG-tagged IGF2BP2 (Figure 4F and Figure S7D). Conversely, the overexpression of *CTBS-GNG5* in the same cell lines markedly reduced IGF2BP2 ubiquitination (Figure 4G and Figure S7E). Collectively, these findings indicate that CTBS-GNG5 attenuates the proteasomal degradation of IGF2BP2 by modulating its polyubiquitination.

2.5. CTBS-GNG5 promotes cell proliferation by regulating IGF2BP2-mediated cell cycle progression.

To elucidate the functional significance of the CTBS-GNG5-IGF2BP2 axis, we knocked down *IGF2BP2* in UM-UC-3 and A549 cells (Figure 5A). CCK-8 and colony

formation assays revealed that *IGF2BP2* knockdown significantly reduced cell viability (Figure 5B-C). We subsequently knocked down *CTBS-GNG5* while overexpressing *IGF2BP2* in the UM-UC-3 and A549 cell lines (Figure 5D). Notably, *IGF2BP2* overexpression rescued the *CTBS-GNG5*-knockdown-mediated suppression of cell proliferation (Figure 5E-G) and alleviated G0/G1 phase cell cycle arrest, accompanied by a corresponding restoration in the proportion of cells in S phase (Figure 5H). These findings collectively indicate that CTBS-GNG5 promotes cell proliferation by modulating IGF2BP2-dependent cell cycle progression in various cellular contexts.

2.6. CTBS-GNG5 modulates the stability of *CDK1*, *TOP2A*, and *CDCA2* mRNAs in an IGF2BP2-dependent manner.

To further elucidate the molecular mechanism underlying CTBS-GNG5-mediated cellular proliferation, we conducted transcriptome sequencing to compare the gene expression profiles of *CTBS-GNG5*- and *IGF2BP2*-silenced UM-UC-3 and A549 cells. Silencing either *CTBS-GNG5* or *IGF2BP2* significantly downregulated a shared set of 99 genes in both UM-UC-3 and A549 cells ($p < 0.05$, |log2-fold change| > 1), including key cell cycle regulators such as *CDK1*, *TOP2A*, and *CDCA2* (Figure 6A-B, Figure S8A). Previous studies have reported that *CDK1*, *TOP2A*, and *CDCA2* are essential for cell cycle progression [22-24]. Kyoto Encyclopedia of Genes and Genomes (KEGG) pathway analysis revealed that these differentially expressed genes are involved primarily in cell cycle regulation, DNA replication, homologous recombination, and cellular senescence (Figure 6C). Furthermore, qRT-PCR analysis revealed significant reductions in *CDK1, TOP2A*, and *CDCA2* expression after *CTBS-GNG5* silencing (Figure 6D). Given the established role of IGF2BP2 in regulating mRNA stability [25], we investigated whether the CTBS-GNG5 fusion protein contributes to the stabilization of target gene transcripts through IGF2BP2. Notably, the overexpression of *IGF2BP2* reversed the down-regulation of target genes induced by *CTBS-GNG5* knockdown at both the mRNA and protein levels (Figure 6E-F). To further assess mRNA stability, actinomycin D treatment was used to monitor the decay of preexisting transcripts. Our

results revealed that silencing *CTBS-GNG5* significantly shortened the half-lives of the *CDK1*, *TOP2A*, and *CDCA2* mRNAs (Figure 6G and Figure S8B). Moreover, *IGF2BP2* overexpression effectively counteracted the destabilizing effect of *CTBS-GNG5* knockdown on target mRNA transcripts (Figure 6H and Figure S8C). Collectively, these data indicate that CTBS-GNG5 regulates the stability of the *CDK1*, *TOP2A*, and *CDCA2* mRNAs in an IGF2BP2-dependent manner (Figure 6I).

3. Discussion

Protein-coding housekeeping genes are well characterized in cells, however, the existence of housekeeping chimeric RNAs remains largely unexplored [5, 16, 26-28]. Our study identifies the chimeric RNA *CTBS-GNG5* as a ubiquitously expressed, housekeeping transcript and elucidates its critical role in regulating cell cycle progression through a novel post-translational mechanism dependent on IGF2BP2. The widespread expression of *CTBS-GNG5* across nearly all normal and malignant tissues challenges the conventional dogma that chimeric RNAs are primarily cancer-specific artifacts. Instead, it positions a subset of these molecules as potential fundamental regulators of cellular homeostasis, a concept that is gaining recognition but still lacks robust functional evidence.

Several chimeric RNAs associated with tumorigenesis or normal physiological processes have been identified in previous studies [10, 13, 29-31]. However, there have been fewer reports on the concurrent expression of housekeeping genes in both tumor and normal tissues [3, 15, 32, 33]. Analysis of sequencing data from the GTEx and TCGA databases revealed that chimeric RNA *CTBS-GNG5* is widely expressed across nearly all normal tissues and malignant tumors, suggesting its potential involvement in fundamental cellular processes [3]. Nevertheless, the mechanisms by which *CTBS-GNG5* influences cellular functions remain largely unclear. In this study, we demonstrated that the housekeeping chimeric RNA *CTBS-GNG5* and its encoded fusion protein are broadly expressed in various tissues and cell types. Furthermore, we developed an antibody specifically targeting the chimeric junction, which selectively

recognizes an epitope across the junction sequence, enabling accurate and reliable detection across multiple platforms, including western blotting, immunohistochemistry, and immunofluorescence. This advancement effectively addresses a persistent challenge in fusion protein research, where shared epitopes between fusion products and their wild-type counterparts often compromise detection specificity.

Previous studies have demonstrated that chimeric RNAs can influence cellular processes through diverse mechanisms, including functioning as long non-coding RNAs [6], encoding fusion proteins [34], or disrupting the expression of parental genes [8]. For example, the *SLC45A3-ELK4* fusion transcript exerts a non-coding regulatory role in prostate cancer cell proliferation [6, 8], whereas the *SLC2A11-MIF*-encoded protein promotes metastasis by stabilizing *PLK1*, *ROBO1*, and *PIK3R3* mRNAs via interaction with PTBP1 [7]. In this study, we show that *CTBS-GNG5* functions primarily through the production of a fusion protein. The parental *CTBS* gene is a glycosidase involved in lysosomal function [35], while *GNG5* is a modulator of G protein-coupled receptor signalling and participates in metabolic and signal transduction pathways [36]. In contrast, the CTBS-GNG5 fusion protein exhibits distinct functional properties associated with cell cycle regulation. This finding underscores the capacity of chimeric RNAs to acquire novel functions that diverge from those of their parental genes, thereby contributing to the regulation of critical biological processes. These results suggest that chimeric RNAs represent an additional mechanism for expanding the functional complexity of the genome without increasing gene number.

The CTBS-GNG5 fusion protein directly interacts with IGF2BP2, an RNA-binding protein essential for post-transcriptional gene regulation, enabling the recognition of N6-methyladenosine-modified RNAs and thereby extending their half-lives [25]. As a key m6A recognition factor, IGF2BP2 enhances mRNA stability and translational efficiency, promoting cell proliferation, malignant transformation, and metabolic regulation in both normal and cancerous cells [37]. In this context, CTBS-GNG5 acts as a molecular scaffold that stabilizes IGF2BP2 by protecting it from proteasomal degradation and augmenting its ability to stabilize transcripts involved in cell cycle

progression.

To elucidate the downstream genes regulated by CTBS-GNG5, transcriptome sequencing was performed across multiple cell lines, leading to the identification of several consistently differentially expressed genes associated with cell cycle regulation, including *CDK1*, *TOP2A*, and *CDCA2*. Subsequent experimental validation confirmed that CTBS-GNG5 modulates their expression by influencing the stability of their corresponding mRNAs. Among them, *CDK1*, a key catalytic subunit of cyclin-dependent kinase complexes, plays a pivotal role in regulating mitotic entry and progression through the phosphorylation of critical substrates involved in spindle assembly and chromosome segregation [22, 38, 39]. *TOP2A* encodes DNA topoisomerase IIα, an enzyme predominantly expressed in proliferating cells that is essential for DNA replication, repair, recombination, and transcription [23]. *CDCA2*, a member of the cell cycle-regulated protein family, has been implicated in the initiation and progression of various malignancies by promoting cell proliferation [24, 40]. Collectively, these CTBS-GNG5-regulated genes are integral components of cell cycle regulatory networks, coordinating orderly transitions between distinct cell cycle phases. In conclusion, we have unveiled a paradigm for a widely expressed chimeric RNA that functions as a central regulator of cell cycle, a core cellular process. The CTBS-GNG5 fusion protein stabilizes IGF2BP2 to enhance the expression of a network of genes driving proliferation, thereby bridging normal cellular physiology and potential malignant transformation (Figure 6I). Our findings argue for a broader re-evaluation of the functional repertoire of chimeric RNAs in normal biology, while the specific tools and mechanisms that we describe offer new clinical translation and applications.

4. Experimental Section

Human tissue samples: This study detected the chimeric RNA *CTBS-GNG5* in both cancerous and adjacent non-tumor tissues obtained from patients at Sun Yat-Sen Memorial Hospital. Sample collection was performed in strict accordance with the ethical principles outlined in the Declaration of Helsinki, and institutional ethical approval was granted by the Ethics Committee of Sun Yat-Sen Memorial Hospital. The

specimens were collected prospectively between January 2010 and February 2023.

TCGA and GTEx platform data analysis: In this study, RNA-seq data from tumor tissues and their matched normal counterparts across various tissue types were obtained from The Cancer Genome Atlas (TCGA) database (https://cancergenome.nih.gov/) and the Genotype-Tissue Expression (GTEx) database (https://www.genome.gov/Funded-Programs-Projects/Genotype-Tissue-Expression-Project). A comprehensive set of bioinformatics analyses was subsequently conducted to assess the expression levels of the chimeric RNA *CTBS-GNG5* in these samples.

Detection of full-length CTBS-GNG5: To determine the full length of the *CTBS-GNG5* transcript, we initially truncated the junction region to 14 base pairs at each end, incorporating reverse complements. Using the AGREP tool, we subsequently conducted a comprehensive search for sequence matches, allowing for zero or two mismatches across all ENCODE datasets. The identified reads were then aligned via BLAT and filtered with a custom program called reps to identify high-confidence genomic mappings. Finally, the alignment coordinates were analysed within an extended genomic region of approximately 300 kb surrounding the predicted chimeric RNA locus.

Nested PCR, agarose gel electrophoresis, and Sanger sequencing: To validate the authenticity of the full-length *CTBS-GNG5* transcript identified through bioinformatics analysis, nested PCR was employed. Initially, a pair of primers was designed to target the two most distal exons, the leftmost and rightmost exons, based on the predicted transcript sequence. The first round of PCR amplification was conducted using cDNA templates derived from multiple cell lines. The first-round PCR products, which were diluted tenfold, were subsequently used as templates for the second round of PCR. In this step, multiple primer pairs were designed to amplify internal exons progressively along the full-length *CTBS-GNG5* transcript, moving from the outermost regions inwards. Each primer pair was tested in separate reactions. The resulting amplicons were analysed via agarose gel electrophoresis. DNA bands corresponding to the expected sizes were excised from the gel and subjected to Sanger sequencing. Sequence analysis confirmed the structure and integrity of the full-length *CTBS-GNG5* transcript.

Cell lines and cell culture: The human bladder cancer cell line UM-UC-3, the human normal bladder epithelial cell line SV-HUC-1, the human non-small cell lung cancer cell line A549, the human hepatoma cell line HepG2, the human prostate cancer cell line PC3, the human breast cancer cell line MDA-MB-231, the normal human prostate stroma cell line WPMY-1, the human normal lung epithelial cell line BEAS-2B, and the human embryonic kidney cell line HEK293T were obtained from the American Type Culture Collection (ATCC). All of the cell lines were maintained in a humidified incubator at 37°C under 5% CO_2. Specifically, UM-UC-3, BEAS-2B, HepG2, MDA-MB-231, WPMY1, and HEK293T cells were cultured in Dulbecco's modified Eagle's medium (DMEM) supplemented with 10% fetal bovine serum (FBS); PC3 and A549 cells were grown in Roswell Park Memorial Institute (RPMI)-1640 medium supplemented with 10% FBS; SV-HUC-1 cells were maintained in Kaighn's modified Ham's F-12 medium (F-12K) supplemented with 10% FBS.

Detection of precursor readthrough mRNA: DNase I was used to remove potential DNA contamination from the isolated RNA. Reverse transcription (RT) was carried out using a reverse primer annealing to the downstream exon adjacent to the splice junction, followed by RT-PCR amplification with primers spanning a fragment of the 5′ region of the gene. Complete DNase I digestion was confirmed by the absence of amplification signal in the control reaction lacking AMV reverse transcriptase.

Preparation of specific antibodies: The polypeptide sequence CEAKSISENGDMPN-KENGD was synthesized via a solid-phase synthesis method. The synthesized polypeptides were subsequently conjugated and used as antigens. Cell fusion was carried out using mouse spleen cells. Hybridoma cells producing specific antibodies were screened for positivity and expanded through culture. Positive hybridoma clones were inoculated into the abdominal cavity of mice to generate sufficient quantities of ascites fluid. Antibody specificity in the cell culture supernatant was evaluated via techniques such as enzyme-linked immunosorbent assay (ELISA). The selected positive clones were utilized for the preparation and purification of monoclonal antibodies.

RNA interference: Small interfering RNA oligonucleotide sequences (siRNAs) specific to *CTBS-GNG5* and *IGF2BP2*, along with a negative control siRNA, were obtained from GenePharma (Shanghai, China) and are listed in Supplementary Table S1. The transfection procedures followed the supplier's guidelines and lipofection protocols were optimized [41]. Briefly, 5 μL of siRNA mixture was combined with 3 μL of Lipofectamine RNAiMAX (Invitrogen, USA) in 200 μL of Opti-MEM (Gibco, USA) and incubated at 25°C for 20 min to form complexes. The mixture was then applied to the cells, which were subsequently cultured for 48 h under standard conditions to assess the effects of the knockdown.

Lentivirus transduction: To achieve targeted gene silencing of *CTBS-GNG5* or *IGF2BP2*, specific short hairpin RNA (shRNA) sequences were subcloned and inserted into the pLKO.1-Puro lentiviral vector, which was optimized for RNA interference applications. In parallel, the open reading frame (ORF) of *CTBS-GNG5* or *IGF2BP2* was incorporated into the pCDH-CMV-MCS-EF1-Puro construct for overexpression studies. Both plasmids were obtained from IGE (Guangzhou, Guangdong, China). A detailed enumeration of all of the shRNA sequences used is presented in Supplementary Table S1. The production of lentiviral particles and subsequent cellular transduction were performed in accordance with standardized methodologies based on established lentiviral delivery systems [42].

RNA isolation, qPCR, and Western blotting: RNA extraction from cells was accomplished via TRIzol reagent (Vazyme, Nanjing, China), followed by quantitative real-time PCR analysis via established methodologies [43, 44]. For reverse transcription, the HiScript III RT SuperMix Kit (Vazyme) was used in strict accordance with the manufacturer's specifications. Subsequent PCR amplification was conducted on a LightCycler 384 platform (Roche) with ChamQ Universal SYBR qPCR Master Mix (Vazyme). Target gene expression levels were determined via the $2^{-\Delta\Delta Ct}$ calculation, and GAPDH was used for normalization; primer sequences are provided in Supplementary Table S2. For western blotting, cellular lysis was performed via RIPA buffer (CWBIO, Beijing, China) containing protease and phosphatase inhibitors

(CWBIO, Beijing, China). Protein quantification was achieved via the Pierce BCA Protein Assay Kit (Invitrogen, Carlsbad, California, USA). Proteins were then separated by SDS–PAGE, transferred onto PVDF membranes (Merck, Burlington, Massachusetts, USA), and blocked prior to overnight incubation at 4°C with primary antibodies against CTBS-GNG5, IGF2BP2, Myc-tag, FLAG-tag, CDCA2, CDK1, TOP2A and GAPDH (refer to Supplementary Table S3). The membranes were subsequently incubated with HRP-conjugated secondary antibodies for 1 hour at 25°C, and protein detection was performed via enhanced chemiluminescence.

Cell proliferation assays: To assess cell proliferation, two complementary methodologies were employed following established protocols: the Cell Counting Kit-8 (CCK-8) assay and colony formation analysis [45]. For CCK-8 quantification, cells were seeded in triplicate within 96-well plates at 2,000 cells per well. After 2 hours of incubation with the Cell Counting Kit-8 reagent (APExBIO, USA), the optical density (OD) was measured at 450 nm via a microplate reader. The colony formation assays involved plating 1,000 cells from the corresponding experimental groups into 6-well plates. Following 10 days of culture, colonies were fixed with 4% paraformaldehyde, stained with 0.1% crystal violet, and quantified based on standardized morphological criteria using ImageJ for image analysis.

Immunohistochemistry (IHC) analysis: Immunohistochemical staining was performed according to established methodologies [46]. Initially, tissue sections were deparaffinized and rehydrated, followed by antigen retrieval through exposure to protease K at 37°C for 15 min. Endogenous peroxidase activity was then suppressed by treatment with 3% H_2O_2 for 10 min at 25°C. The primary antibodies (detailed in Supplementary Table S3) were subsequently applied and incubated with the samples overnight at 4°C. After three rinses with PBS, biotin-conjugated secondary antibodies were introduced for 1h at 25°C, and chromogenic visualization was achieved via DAB substrate (ZSGB-BIO, Beijing, China). Finally, nuclear counterstaining was conducted with hematoxylin. The quantitative evaluation of the stained samples was performed according to previously described protocols [7]. Two blinded pathologists assessed

protein expression via a standardized scoring system. In cases where there was a significant disparity in the score results for the same tissue, rescoring was conducted until a consensus was reached. The specific scoring method employed was as follows: First, all sections were examined for staining intensity and categorized into four levels. The percentage of positively stained tumor cells was scored as follows: 0 (no positive staining), 1 ($\leqslant$10% positive), 2 (>10% to $\leqslant$30% positive), 3 (>30% to $\leqslant$70% positive), or 4 (>70% positive). The staining intensity was graded as follows: 1 (no staining), 2 (weak staining, light yellow), 3 (moderate staining, brown), or 4 (strong staining, brown red). The staining index (SI) was calculated by multiplying the proportion of positively stained tumor cells by the corresponding intensity score for a range of possible scores, which included 0, 1, 2, 3, 4, 6, 8, 9, 12, and 16.

Flow cytometry analysis: Apoptosis was quantified via an Annexin V-FITC/PI detection kit (A211-01, Vazyme, Nanjing, China), wherein FITC-conjugated Annexin V binds to externalized phosphatidylserine on apoptotic cells, and propidium iodide (PI) stains nuclei in late-stage apoptosis or necrosis, following standard protocols [47]. Concurrently, the distribution across cell cycle phases was analysed with a Cell Cycle Detection Kit (KGA512, KeyGEN, Nanjing, China), which employs flow cytometry (BD Biosciences, San Jose, CA, USA) with PI labelling for DNA content assessment to monitor cellular growth dynamics.

Tumor xenograft model: All procedures involving animals received ethical clearance from the Institutional Animal Care and Use Committee at Sun Yat-Sen University. We obtained male BALB/c nude mice (aged 4–5 weeks) from the university's Experimental Animal Center and maintained them under specific pathogen-free (SPF) conditions. A suspension containing 3×10^6 UM-UC-3, HepG2, or MDA-MB-231 cells was administered subcutaneously below the right scapular region of each mouse. Following inoculation, the injection area was examined daily, and subcutaneous tumor dimensions were quantified every three days. Upon meeting predefined humane endpoints, the mice were euthanized via cervical dislocation. Excised tumors underwent photographic documentation, measurement, weighing, and fixation in 4% paraformaldehyde.

Following fixation, the samples were paraffin-embedded, and the largest cross-section was isolated for downstream analyses. Histopathological evaluations, including hematoxylin and eosin (H&E) staining and Ki67 immunohistochemistry, were performed on these sections [48].

Coimmunoprecipitation (Co-IP) and mass spectrometry (MS) analysis: For coimmunoprecipitation, the Pierce Crosslink Magnetic Co-IP Kit (Thermo Scientific, USA) was utilized according to the manufacturer's protocol and prior methodology [49]. The cell lysates were incubated in IP lysis buffer supplemented with protease inhibitors, followed by overnight rotation at 4°C with anti-Myc-tag, anti-IGF2BP2, or IgG antibodies (Supplementary Table S3). Protein–antibody complexes were captured by adding Protein A&G magnetic beads and rotating for 2 hours. The beads were washed three times, and the bound proteins were eluted by boiling at 95°C for 10 minutes prior to western blotting. Mass spectrometry was conducted at the Bioinformatics and Omics Centre of Sun Yat-Sen Memorial Hospital.

Immunofluorescence (IF) staining: Immunofluorescence staining was performed as previously described [50]. In brief, the cells were seeded into confocal dishes and fixed with 4% paraformaldehyde for 15 min, followed by permeabilization with 0.5% Triton X-100 for 10 min. The cells were subsequently blocked with 5% bovine serum albumin (BSA) for 30 min and then treated overnight at 4°C with primary antibodies diluted in blocking buffer. The primary antibodies used to target Myc-tag and IGF2BP2 are detailed in Supplementary Table S3. After three washes with PBS, the cells were incubated with secondary antibodies for 1 hour at room temperature. Nuclear counterstaining was achieved via incubation with DAPI (Solarbio, Beijing, China) for 5 min, and images were acquired via a Zeiss confocal microscope (Munich, Germany).

RNA sequencing analysis: The cells were transfected with siRNAs specific to *CTBS-GNG5* or *IGF2BP2*, along with negative control siRNA, for 48 hours. Total RNA was then isolated via vigorous pipetting and phase separation using TRIzol reagent (Vazyme, Nanjing, China). Following ethanol precipitation and quality verification, the RNA samples were subjected to transcriptome profiling via high-throughput sequencing. Libraries were prepared and sequenced on an Illumina platform by NovoGene

Technology (Beijing, China) via paired-end sequencing technology. Differential gene expression between the control and knockdown groups was subsequently analysed via a computational pipeline for RNA-seq data. All primary RNA-seq data were uploaded to Genome Sequence Archive (GSA: HRA013901) (https://ngdc.cncb.ac.cn/gsa/)

Statistics: All statistical graphs and analyses were generated using GraphPad Prism 10.0 software, with error bars representing standard deviation (SD). The statistical significance of differences between groups was assessed using unpaired or paired Student's t tests, one-way analysis of variance (ANOVA), or 2-way ANOVA. Additional statistical analyses were conducted using R (v4.4.1).

Ethics approval: Ethical consent for this study was obtained from the Sun Yat-Sen Memorial Hospital Committees for Ethical Review of Research involving Human Subjects (SYSKY-2022-392-0). All human tissue samples were obtained from patients who provided written informed consent. Ethical approval for this study was granted by the Sun Yat-Sen University Committees for Ethical Review of Research Involving Animal Experiments (AP20250286).

Acknowledgements

This study was supported by the National Natural Science Foundation of China (82322056, 82473416, 82173230, 82273421), the Science and Technology Program of Guangzhou (2023A03J0718,2024B03J12342024A04J6558), Guangdong Provincial Clinical Research Centre for Urological Diseases (2020B1111170006), Guangdong Science and Technology Department (2020B1212060018, 2018B030317001, 2017B030314026), Guangdong Basic and Applied Basic Research Foundation (2023A1515110957, 2023A1515110515), the Fostering Program for NSFC Young Applicants (Tulip Talent Training Program) of Sun Yat-sen University Cancer Center (No. 2025yfd11), the Guangdong Medical Science and Technology Research Program (Grant No. B2025253), and the Sun Yat-sen Pilot Scientific Research Fund (Grant No. YXQH202504).

Conflicts of interest

The authors declare that they have no conflicts of interest.

Author contributions

X.C., H.L., and J.H. designed the study. L.C., J.T.Z., X.L.L. and C.W.Y. conducted the main experiments and performed the data analysis. F.J.Q. provided guidance on the identification and validation of the chimeric RNA. Y.H.H., M.H. and R.H.X. analysed the clinical characteristics. S.L. and J.E. performed the bioinformatic analysis, and S.M.P. and S.T.C. conducted the *in vitro* and *in vivo* functional experiments. B.Q.H., H.F.W., and T.X.L. conducted the statistical analyses. J.H., H.L., and X.C. wrote and reviewed the manuscript. All the authors read and approved the final manuscript. The order of authorship among co-first authors was determined based on their relative contributions.

Data availability Statement

The descriptions of the data mining methods used in the TCGA study are provided in the MATERIALS AND METHODS. The raw RNA-seq data can be obtained from the GSA database (HRA013901).

Keywords

Chimeric RNA, Fusion Protein, Cell Cycle, mRNA Stability, IGF2BP2, Ubiquitination, housekeeping protein

References

[1] X. Shi, S. Singh, E. Lin, H. Li, Chimeric RNAs in cancer, Advances in clinical chemistry, 100 (2021) 1-35.

[2] W. Wang, X. Zhang, N. Zhao, Z.H. Xu, K. Jin, Z.B. Jin, RNA fusion in human retinal development, eLife, 13 (2024).

[3] M. Babiceanu, F. Qin, Z. Xie, Y. Jia, K. Lopez, N. Janus, L. Facemire, S. Kumar, Y. Pang, Y. Qi, I.M. Lazar, H. Li, Recurrent chimeric fusion RNAs in non-cancer tissues and cells, Nucleic acids research, 44 (2016) 2859-2872.

[4] K. Chwalenia, L. Facemire, H. Li, Chimeric RNAs in cancer and normal physiology, Wiley

interdisciplinary reviews. RNA, 8 (2017).
[5] D. Zhu, S. Singh, X. Chen, Z. Zheng, J. Huang, T. Lin, H. Li, The landscape of chimeric RNAs in bladder urothelial carcinoma, The international journal of biochemistry & cell biology, 110 (2019) 50-58.
[6] F. Qin, Y. Zhang, J. Liu, H. Li, SLC45A3-ELK4 functions as a long non-coding chimeric RNA, Cancer letters, 404 (2017) 53-61.
[7] L. Cheng, C. Yang, J. Lu, M. Huang, R. Xie, S. Lynch, J. Elfman, Y. Huang, S. Liu, S. Chen, B. He, T. Lin, H. Li, X. Chen, J. Huang, Oncogenic SLC2A11-MIF fusion protein interacts with polypyrimidine tract binding protein 1 to facilitate bladder cancer proliferation and metastasis by regulating mRNA stability, MedComm, 5 (2024) e685.
[8] D.S. Rickman, D. Pflueger, B. Moss, V.E. VanDoren, C.X. Chen, A. de la Taille, R. Kuefer, A.K. Tewari, S.R. Setlur, F. Demichelis, M.A. Rubin, SLC45A3-ELK4 is a novel and frequent erythroblast transformation-specific fusion transcript in prostate cancer, Cancer research, 69 (2009) 2734-2738.
[9] S.A. Tomlins, D.R. Rhodes, S. Perner, S.M. Dhanasekaran, R. Mehra, X.W. Sun, S. Varambally, X. Cao, J. Tchinda, R. Kuefer, C. Lee, J.E. Montie, R.B. Shah, K.J. Pienta, M.A. Rubin, A.M. Chinnaiyan, Recurrent fusion of TMPRSS2 and ETS transcription factor genes in prostate cancer, Science (New York, N.Y.), 310 (2005) 644-648.
[10] B.X. Li, L.L. David, L.E. Davis, X. Xiao, Protein arginine methyltransferase 5 is essential for oncogene product EWSR1-ATF1-mediated gene transcription in clear cell sarcoma, The Journal of biological chemistry, 298 (2022) 102434.
[11] M.Y. Ou, Q. Xiao, X.C. Ju, P.M. Zeng, J. Huang, A.L. Sheng, Z.G. Luo, The CTNNBIP1-CLSTN1 fusion transcript regulates human neocortical development, Cell reports, 35 (2021) 109290.
[12] C. Chen, F. Qin, S. Singh, Y. Tang, H. Li, CTNNBIP1-CLSTN1 functions as a housekeeping chimeric RNA and regulates cell proliferation through SERPINE2, Cell death discovery, 9 (2023) 369.
[13] Y. Tang, F. Qin, A. Liu, H. Li, Recurrent fusion RNA DUS4L-BCAP29 in non-cancer human tissues and cells, Oncotarget, 8 (2017) 31415-31423.
[14] H.P. Kim, G.A. Cho, S.W. Han, J.Y. Shin, E.G. Jeong, S.H. Song, W.C. Lee, K.H. Lee, D. Bang, J.S. Seo, J.I. Kim, T.Y. Kim, Novel fusion transcripts in human gastric cancer revealed by transcriptome analysis, Oncogene, 33 (2014) 5434-5441.
[15] Y. Tang, S. Ma, X. Wang, Q. Xing, T. Huang, H. Liu, Q. Li, Y. Zhang, K. Zhang, M. Yao, G.L. Yang, H. Li, X. Zang, B. Yang, F. Guan, Identification of chimeric RNAs in human infant brains and their implications in neural differentiation, The international journal of biochemistry & cell biology, 111 (2019) 19-26.
[16] S. Singh, F. Qin, S. Kumar, J. Elfman, E. Lin, L.P. Pham, A. Yang, H. Li, The landscape of chimeric RNAs in non-diseased tissues and cells, Nucleic acids research, 48 (2020) 1764-1778.
[17] Y. Matsumoto, T. Tsukamoto, Y. Chinen, Y. Shimura, N. Sasaki, H. Nagoshi, R. Sato, H. Adachi, M. Nakano, S. Horiike, J. Kuroda, T. Taki, K. Tashiro, M. Taniwaki, Detection of novel and recurrent conjoined genes in non-Hodgkin B-cell lymphoma, Journal of clinical and experimental hematopathology : JCEH, 61 (2021) 71-77.
[18] J. Zhou, X. Guan, E. Xu, J. Zhou, R. Xiong, Q. Yang, Chimeric RNA RRM2-C2orf48 plays an oncogenic role in the development of NNK-induced lung cancer, iScience, 26 (2023) 105708.
[19] C.C. Liu, J. Veeraraghavan, Y. Tan, J.A. Kim, X. Wang, S.K. Loo, S. Lee, Y. Hu, X.S. Wang, A Novel Neoplastic Fusion Transcript, RAD51AP1-DYRK4, Confers Sensitivity to the MEK Inhibitor

Trametinib in Aggressive Breast Cancers, Clinical cancer research : an official journal of the American Association for Cancer Research, 27 (2021) 785-798.

[20] B. Dharavath, A. Butle, A. Chaudhary, A. Pal, S. Desai, A. Chowdhury, R. Thorat, P. Upadhyay, S. Nair, A. Dutt, Recurrent UBE3C-LRP5 translocations in head and neck cancer with therapeutic implications, NPJ precision oncology, 8 (2024) 63.

[21] P. Han, R.H. Chen, F. Wang, J.Y. Zeng, S.T. Yu, L.H. Xu, Q. Cai, F.Y. Liang, T.L. Xia, Z.R. Lin, Q. Zhong, X.M. Huang, Novel chimeric transcript RRM2-c2orf48 promotes metastasis in nasopharyngeal carcinoma, Cell death & disease, 8 (2017) e3047.

[22] B. Xie, S. Wang, N. Jiang, J.J. Li, Cyclin B1/CDK1-regulated mitochondrial bioenergetics in cell cycle progression and tumor resistance, Cancer letters, 443 (2019) 56-66.

[23] K. Zhang, X. Zheng, Y. Sun, X. Feng, X. Wu, W. Liu, C. Gao, Y. Yan, W. Tian, Y. Wang, TOP2A modulates signaling via the AKT/mTOR pathway to promote ovarian cancer cell proliferation, Cancer biology & therapy, 25 (2024) 2325126.

[24] X. Lin, Z. Zou, J. Zhong, T. Wang, W. Ma, T. Hu, W. Sun, Y. Xu, A.M.M. Eggermont, Y. Chen, The Role of CDCA2 in tumor genesis, prognosis and future treatments, European journal of cancer (Oxford, England : 1990), 211 (2024) 114308.

[25] J. Wang, L. Chen, P. Qiang, The role of IGF2BP2, an m6A reader gene, in human metabolic diseases and cancers, Cancer cell international, 21 (2021) 99.

[26] A. Biswas, Y. Rajesh, S. Das, I. Banerjee, N. Kapoor, P. Mitra, M. Mandal, Therapeutic targeting of RBPJ, an upstream regulator of ETV6 gene, abrogates ETV6-NTRK3 fusion gene transformations in glioblastoma, Cancer letters, 544 (2022) 215811.

[27] H. Wu, S. Singh, Z. Xie, X. Li, H. Li, Landscape characterization of chimeric RNAs in colorectal cancer, Cancer letters, 489 (2020) 56-65.

[28] P. Wu, S. Yang, S. Singh, F. Qin, S. Kumar, L. Wang, D. Ma, H. Li, The Landscape and Implications of Chimeric RNAs in Cervical Cancer, EBioMedicine, 37 (2018) 158-167.

[29] X. Shi, L. Facemire, S. Singh, S. Kumar, R. Cornelison, C. Liang, F. Qin, A. Liu, S. Lin, Y. Tang, J. Elfman, T. Manley, T. Bullock, D.M. Haverstick, P. Wu, H. Li, UBA1-CDK16 : A Sex-Specific Chimeric RNA and Its Role in Immune Sexual Dimorphism, bioRxiv : the preprint server for biology, (2024).

[30] F. Qin, Y. Song, Y. Zhang, L. Facemire, H. Frierson, H. Li, Role of CTCF in Regulating SLC45A3-ELK4 Chimeric RNA, PloS one, 11 (2016) e0150382.

[31] T. Velusamy, N. Palanisamy, S. Kalyana-Sundaram, A.A. Sahasrabuddhe, C.A. Maher, D.R. Robinson, D.W. Bahler, T.T. Cornell, T.E. Wilson, M.S. Lim, A.M. Chinnaiyan, K.S. Elenitoba-Johnson, Recurrent reciprocal RNA chimera involving YPEL5 and PPP1CB in chronic lymphocytic leukemia, Proceedings of the National Academy of Sciences of the United States of America, 110 (2013) 3035-3040.

[32] S.M. Yun, K. Yoon, S. Lee, E. Kim, S.H. Kong, J. Choe, J.M. Kang, T.S. Han, P. Kim, Y. Choi, S. Jho, H. Yoo, J. Bhak, H.K. Yang, S.J. Kim, PPP1R1B-STARD3 chimeric fusion transcript in human gastric cancer promotes tumorigenesis through activation of PI3K/AKT signaling, Oncogene, 33 (2014) 5341-5347.

[33] S. Nagasawa, K. Ikeda, D. Shintani, C. Yang, S. Takeda, K. Hasegawa, K. Horie, S. Inoue, Identification of a Novel Oncogenic Fusion Gene SPON1-TRIM29 in Clinical Ovarian Cancer That Promotes Cell and Tumor Growth and Enhances Chemoresistance in A2780 Cells, International journal of molecular sciences, 23 (2022).

[34] L. Wang, X. Xiong, Z. Yao, J. Zhu, Y. Lin, W. Lin, K. Li, X. Xu, Y. Guo, Y. Chen, Y. Pan, F. Zhou, J.

Fan, Y. Chen, S. Gao, S.C. Jim Yeung, H. Zhang, Chimeric RNA ASTN2-PAPPA(as) aggravates tumor progression and metastasis in human esophageal cancer, Cancer letters, 501 (2021) 1-11.

[35] M. Di Rosa, C. Sanfilippo, M. Libra, G. Musumeci, L. Malaguarnera, Different pediatric brain tumors are associated with different gene expression profiling, Acta histochemica, 117 (2015) 477-485.

[36] B. Yang, Z.Y. Han, W.J. Wang, Y.B. Ma, S.H. Chu, GNG5 is an unfavourable independent prognostic indicator of gliomas, Journal of cellular and molecular medicine, 24 (2020) 12873-12878.

[37] H. Weng, F. Huang, Z. Yu, Z. Chen, E. Prince, Y. Kang, K. Zhou, W. Li, J. Hu, C. Fu, T. Aziz, H. Li, J. Li, Y. Yang, L. Han, S. Zhang, Y. Ma, M. Sun, H. Wu, Z. Zhang, M. Wunderlich, S. Robinson, D. Braas, J.T. Hoeve, B. Zhang, G. Marcucci, J.C. Mulloy, K. Zhou, H.F. Tao, X. Deng, D. Horne, M. Wei, H. Huang, J. Chen, The m(6)A reader IGF2BP2 regulates glutamine metabolism and represents a therapeutic target in acute myeloid leukemia, Cancer cell, 40 (2022) 1566-1582.e1510.

[38] J.Y. Chotiner, D.J. Wolgemuth, P.J. Wang, Functions of cyclins and CDKs in mammalian gametogenesis†, Biology of reproduction, 101 (2019) 591-601.

[39] F. Faienza, F. Polverino, G. Rajendraprasad, G. Milletti, Z. Hu, B. Colella, D. Gargano, F. Strappazzon, S. Rizza, M.V. Vistesen, Y. Luo, M. Antonioli, V. Cianfanelli, C. Ferraina, G.M. Fimia, G. Filomeni, D. De Zio, J. Dengjel, M. Barisic, G. Guarguaglini, S. Di Bartolomeo, F. Cecconi, AMBRA1 phosphorylation by CDK1 and PLK1 regulates mitotic spindle orientation, Cellular and molecular life sciences : CMLS, 80 (2023) 251.

[40] J. Wang, X. Liu, H. Chu, J. Chen, Cell division cycle associated 2 (CDCA2) upregulation promotes the progression of hepatocellular carcinoma in a p53-dependant manner, PeerJ, 10 (2022) e13535.

[41] R. Xie, L. Cheng, M. Huang, L. Huang, Z. Chen, Q. Zhang, H. Li, J. Lu, H. Wang, Q. Zhou, J. Huang, X. Chen, T. Lin, NAT10 Drives Cisplatin Chemoresistance by Enhancing ac4C-Associated DNA Repair in Bladder Cancer, Cancer research, 83 (2023) 1666-1683.

[42] M. Huang, W. Dong, R. Xie, J. Wu, Q. Su, W. Li, K. Yao, Y. Chen, Q. Zhou, Q. Zhang, W. Li, L. Cheng, S. Peng, S. Chen, J. Huang, X. Chen, T. Lin, HSF1 facilitates the multistep process of lymphatic metastasis in bladder cancer via a novel PRMT5-WDR5-dependent transcriptional program, Cancer communications (London, England), 42 (2022) 447-470.

[43] H. Zhan, H. Wang, B. Pan, J. Lu, K. Xiao, J. Lai, Z. Chen, K. Jie, S. Chen, H. Li, T. Lin, X. Chen, Reprogramming the tumor microenvironment with c-MYC-based gene circuit platform to enhance specific cancer immunotherapy, Nature communications, 16 (2025) 7983.

[44] J. Wu, M. Huang, W. Dong, Y. Chen, Q. Zhou, Q. Zhang, J. Zheng, Y. Liu, Y. Zhang, S. Liu, C. Yang, S. Chen, J. Huang, T. Lin, X. Chen, SUMO E3 ligase MUL1 inhibits lymph node metastasis of bladder cancer by mediating mitochondrial HSPA9 translocation, International journal of biological sciences, 20 (2024) 3986-4006.

[45] Y. Fang, L. Cheng, M. Huang, Y. Cao, Q. Zou, J. Cai, Y. Zhang, Y. Xia, H. Huang, X. Chen, Q. Cai, Heat shock factor 1 promotes proliferation and chemoresistance in diffuse large B-cell lymphoma by enhancing the cell cycle and DNA repair, Cell death & disease, 16 (2025) 533.

[46] H. Wang, H. Zhan, B. Pan, L. Zeng, Z. Chen, S. Liu, Q. Zhang, X. Hong, J. Lu, X. Lin, X. Zhao, J. Lai, K. Jie, Y. Li, J. Zhong, S. Peng, S. Chen, C. Chen, W. Zhong, S. Wu, Y. Pan, T. Lin, X. Chen, Engineering CRISPR System-Based Bacterial Outer Membrane Vesicle Potentiates T Cell Immunity for Enhanced Cancer Immunotherapy, Advanced materials (Deerfield Beach, Fla.), (2025) e2501565.

[47] C. Zhang, S. Liu, J. Zhang, J. Lu, Z. Chen, B. Pan, C. Liu, M. Huang, H. Zhan, H. Wang, S. Chen, K. Jie, B. He, J. Wu, Y. Li, H. Wang, J. Zhao, Q. Zhang, X. Chen, A Multifunctional Fe-EGCG@RSL3 Nanomedicine Synergizes Ferroptosis Induction and Tumor Microenvironment Remodeling for Enhanced Bladder Cancer Immunotherapy, Research (Washington, D.C.), 8 (2025) 0735.

[48] Q. Zhang, S. Liu, H. Wang, K. Xiao, J. Lu, S. Chen, M. Huang, R. Xie, T. Lin, X. Chen, ETV4 Mediated Tumor-Associated Neutrophil Infiltration Facilitates Lymphangiogenesis and Lymphatic Metastasis of Bladder Cancer, Advanced science (Weinheim, Baden-Wurttemberg, Germany), 10 (2023) e2205613.

[49] K. Xiao, S. Peng, J. Lu, T. Zhou, X. Hong, S. Chen, G. Liu, H. Li, J. Huang, X. Chen, T. Lin, UBE2S interacting with TRIM21 mediates the K11-linked ubiquitination of LPP to promote the lymphatic metastasis of bladder cancer, Cell death & disease, 14 (2023) 408.

[50] R. Xie, X. Chen, L. Cheng, M. Huang, Q. Zhou, J. Zhang, Y. Chen, S. Peng, Z. Chen, W. Dong, J. Huang, T. Lin, NONO Inhibits Lymphatic Metastasis of Bladder Cancer via Alternative Splicing of SETMAR, Molecular therapy : the journal of the American Society of Gene Therapy, 29 (2021) 291-307.

Figure Legends

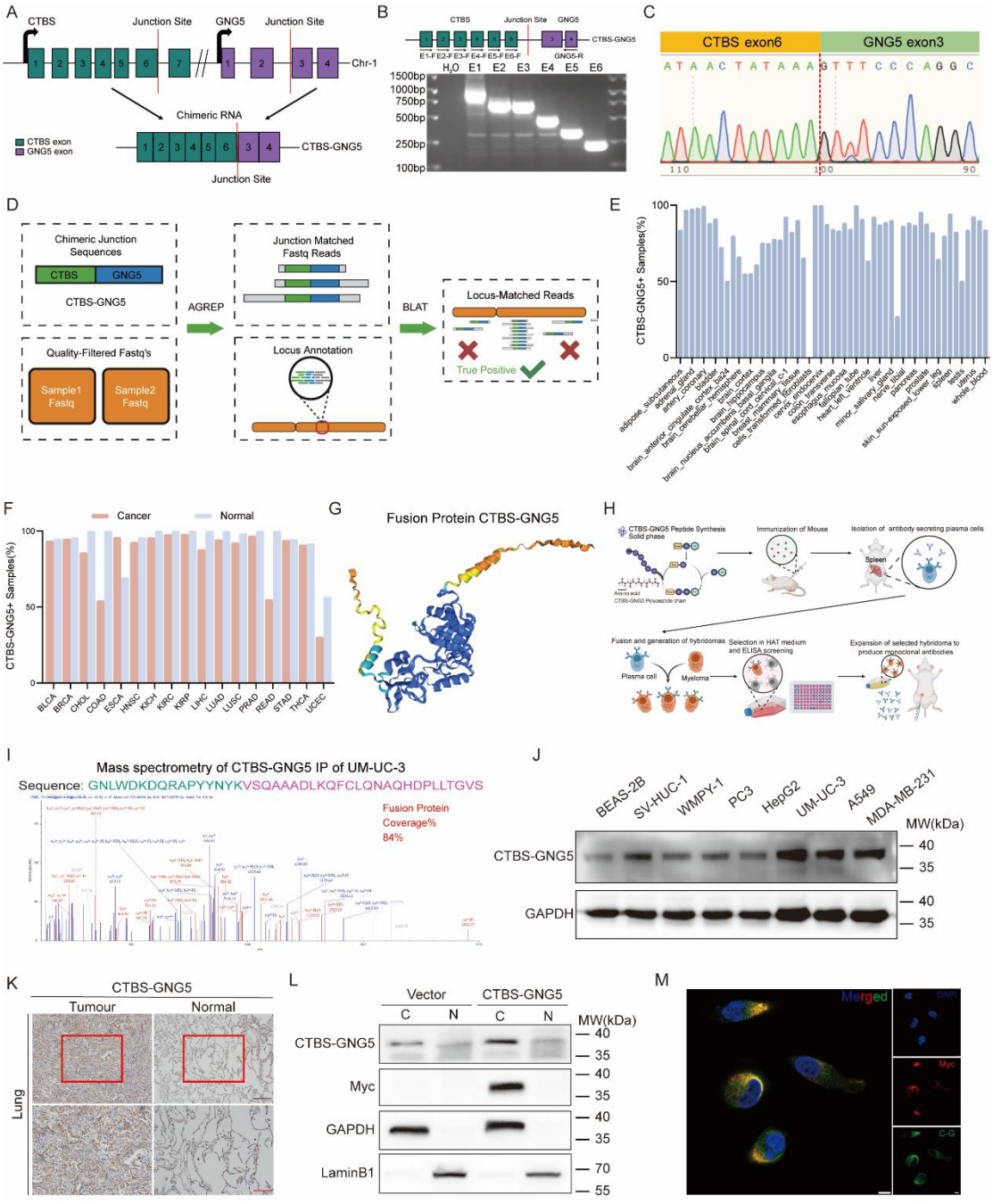

Figure 1. Characterization of the chimeric RNA *CTBS-GNG5* and its fusion protein are widely expressed.

(A) Structure of the *CTBS-GNG5* fusion isoform is depicted, with blocks representing exons and lines representing introns or the intergenic region. (B) Top: Diagram showing the variants of *CTBS-GNG5* mRNA and the primers used for RT–PCR detection of exon 1 (primer E1), exon 2 (primer E2), exon 3 (primer E3), exon 4 (primer E4), exon

5 (primer E5), and exon 6 (primer E6). Bottom: Gel image of RT-PCR product of *CTBS-GNG5* in UM-UC-3 cells. (C) Sanger sequencing results of *CTBS-GNG5*, with the junction indicated by a red dashed line. (D) The flowchart illustrates the comprehensive analysis of full-length *CTBS-GNG5*. (E-F) Proportion of samples positive for chimeric RNA *CTBS-GNG5* transcripts detected in samples from the GTEx (E) and TCGA (F) databases. Red bars in (F) indicate tumor tissue and blue indicates normal matched tissue. (G) Schematic representation of the predicted three-dimensional spatial structure of the fusion protein CTBS-GNG5 generated by AlphaFold3. (H) Flowchart for the preparation of the CTBS-GNG5 fusion protein-specific monoclonal antibody. (I) IP–MS identification of the amino acids in the chimeric region of CTBS-GNG5 and assessment of fusion protein coverage in UM-UC-3 cells. (J) Western blotting was employed to verify the expression of the CTBS-GNG5 fusion protein in both normal and lung cancer cell lines. (K) Immunohistochemistry was used to verify the expression of the CTBS-GNG5 fusion protein in normal and lung cancer tissues. Scale bars indicate 50 μm (black) and 25 μm (red). (L) Nuclear fractionation followed by western blotting detected CTBS-GNG5-Myc abundance in both the nuclear (N) and cytoplasmic (C) compartments, with GAPDH and Lamin B1 serving as internal controls for cytoplasmic and nuclear fraction separation, respectively. (M) Representative IF images demonstrating the colocalization of CTBS-GNG5-Myc in the cytoplasm of UM-UC-3 cells. Blue indicates nuclei, green indicates CTBS-GNG5, and red indicates Myc.

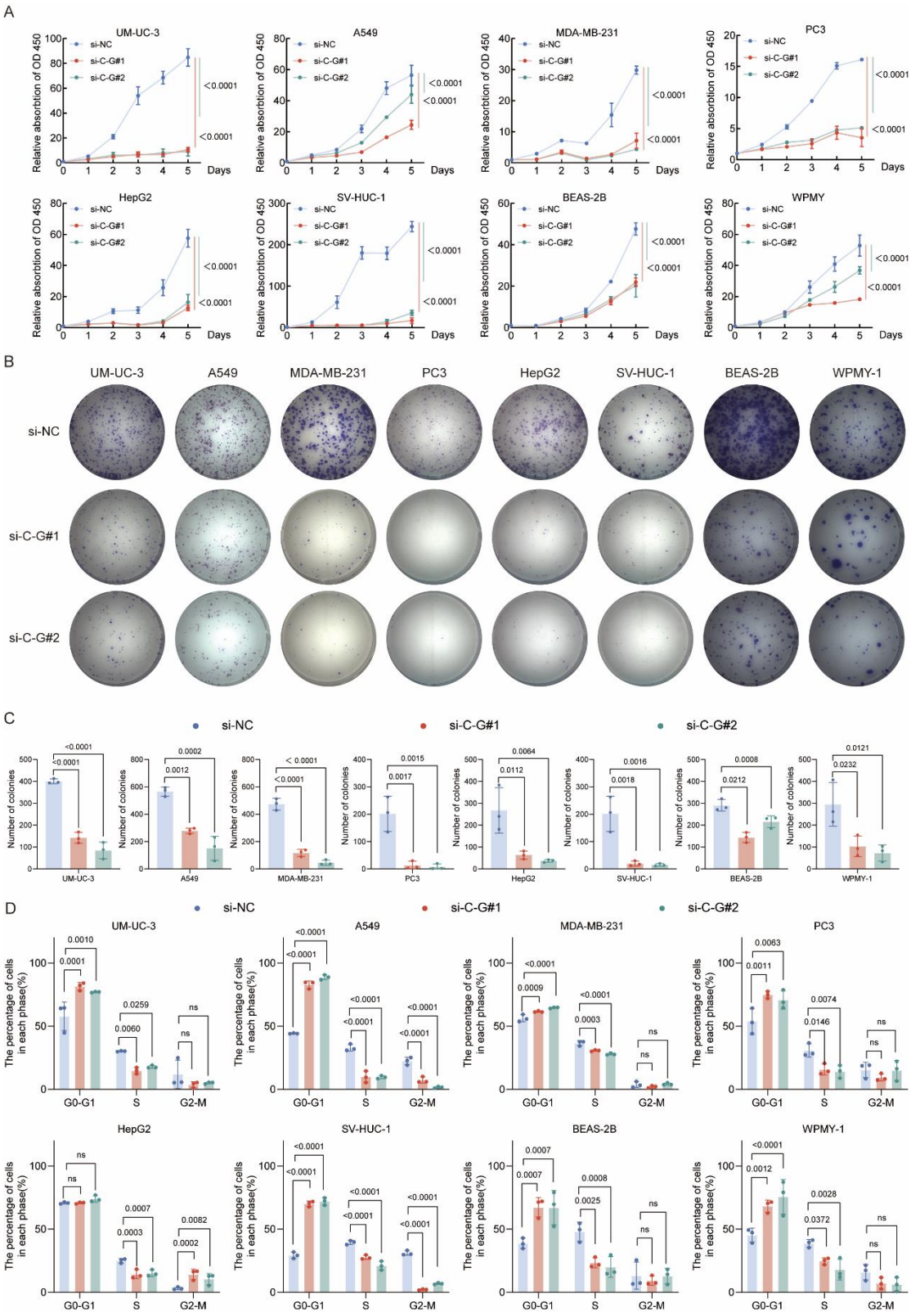

Figure 2. Knockdown of *CTBS-GNG5* inhibited the proliferation of both tumor and normal cells *in vitro.*

(A) Cell viability, as assessed by the CCK-8 assay, was evaluated in UM-UC-3, A549, MDA-MB-231, PC3, HepG2, SV-HUC-1, BEAS-2B, and WPMY-1 cell lines following *CTBS-GNG5* knockdown. (B-C) Representative images (B) and quantification (C) of colony formation assays were obtained for UM-UC-3, A549, MDA-MB-231, PC3, HepG2, SV-HUC-1, BEAS-2B, and WPMY-1 cell lines following *CTBS-GNG5* knockdown. (D) The percentages (%) of cell populations at different stages of the cell cycle are presented after *CTBS-GNG5* knockdown in UM-UC-3, A549, MDA-MB-231, PC3, HepG2, SV-HUC-1, BEAS-2B, and WPMY-1 cell lines. The data are expressed as the means ± SDs. Statistical significance was determined by one-way ANOVA with Tukey's post hoc test (C), and two-way ANOVA with Tukey's post hoc test (A, D). ns indicates not statistically significant.

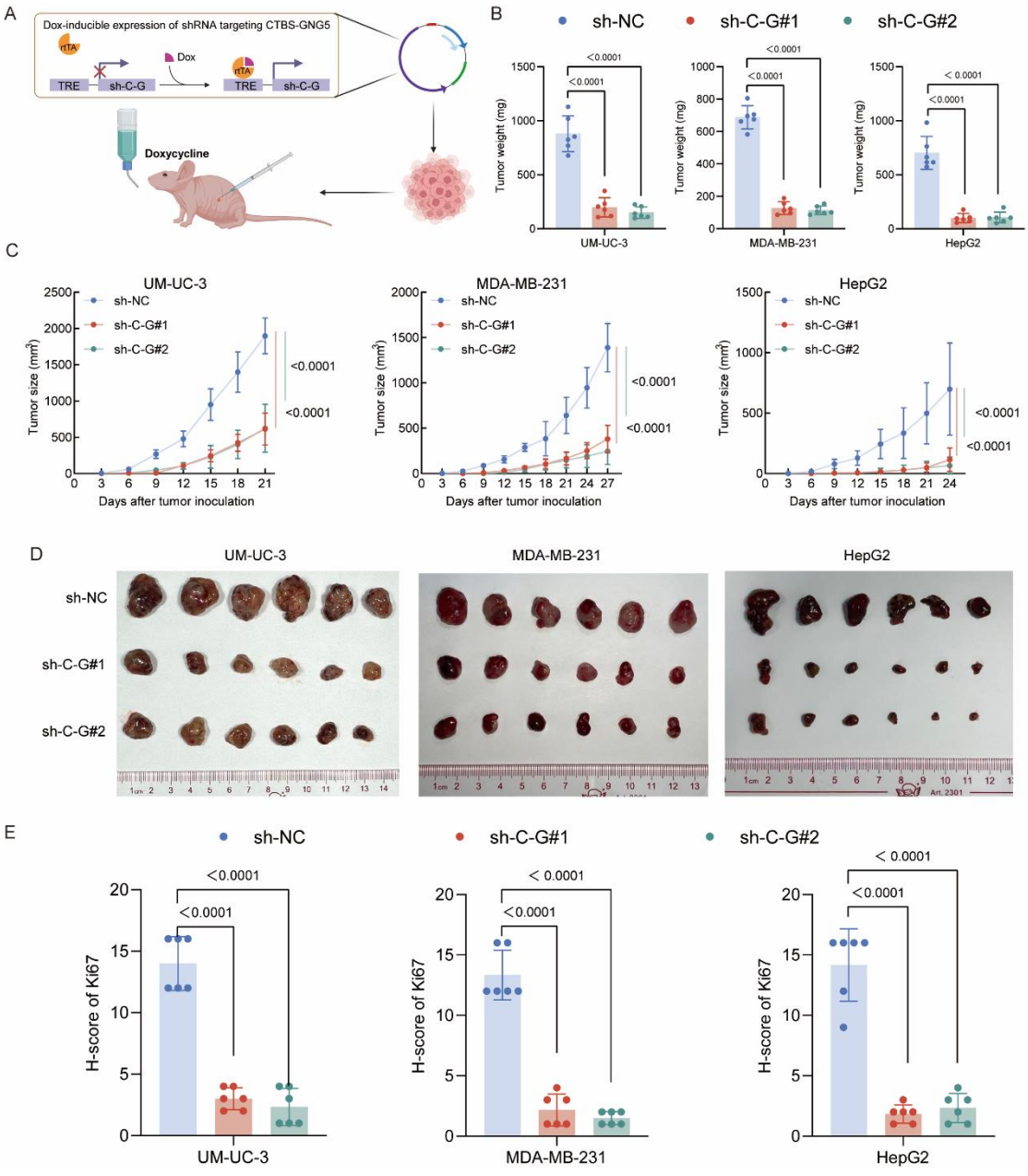

744

745 **Figure 3. Knockdown of *CTBS-GNG5* inhibited the proliferation of tumor cells *in***
746 ***vivo*.**

747 (A) Schematic representation of an animal model of doxycycline-induced sh-*CTBS-*
748 *GNG5* expression. (B) Weights (in mg) of tumors with *CTBS-GNG5* knockdown after
749 surgical dissection. (C) The growth of UM-UC-3, HepG2, and MDA-MB-231 tumors
750 following *CTBS-GNG5* knockdown was monitored at three-day intervals, and tumor
751 growth curves were generated accordingly. The tumor volume data from six mice are
752 expressed as the mean ± standard deviation (S.D.). (D) Representative images of

subcutaneous tumors in which *CTBS-GNG5* was knocked down. (E) Histogram of the H-scores of Ki67 tumors with *CTBS-GNG5* knockdown. The data are expressed as the means ± SDs. Statistical significance was determined by one-way ANOVA with Tukey's post hoc test (B,E), and two-way ANOVA with Tukey's post hoc test (C).

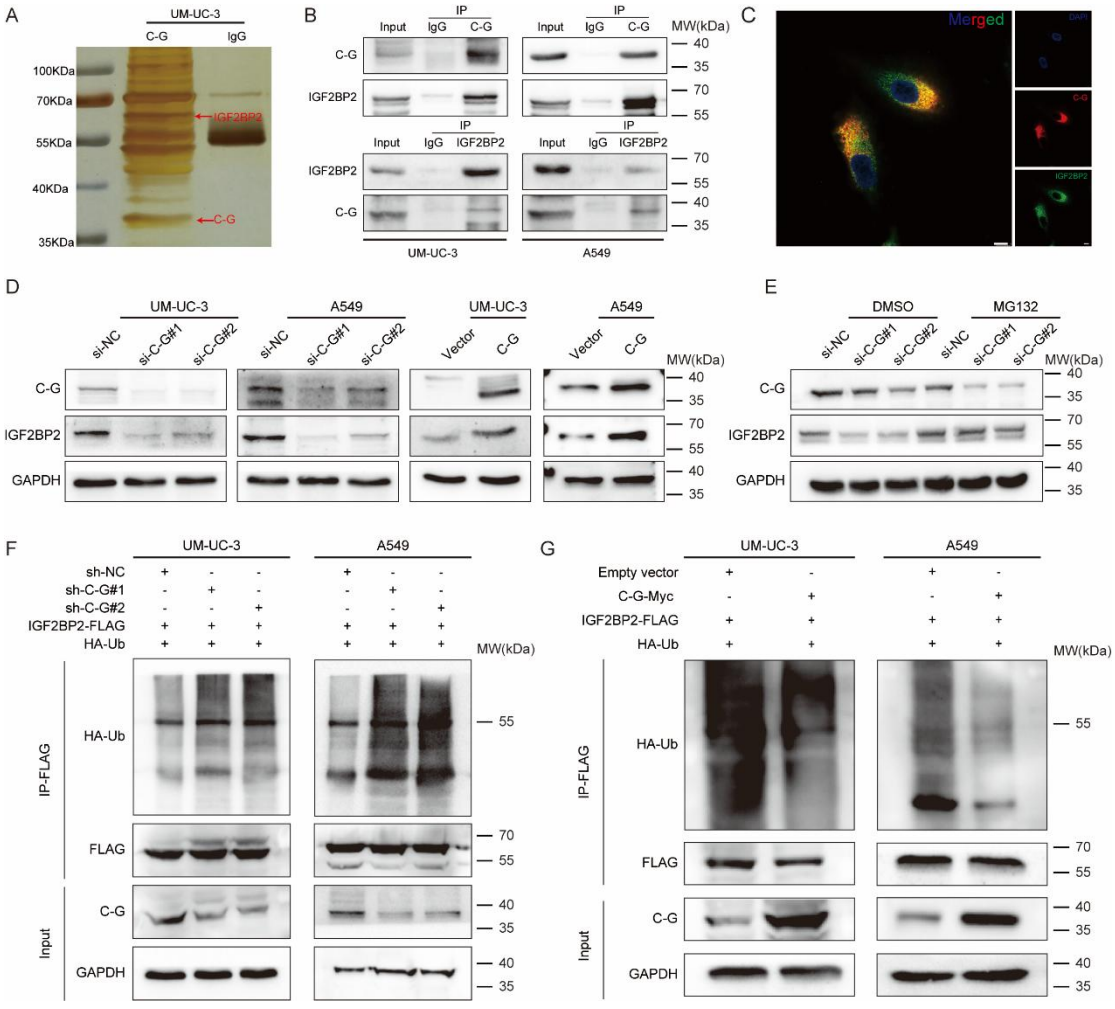

Figure 4. The CTBS-GNG5 fusion protein stabilizes IGF2BP2 through the inhibition of ubiquitin-mediated degradation.

(A) Coimmunoprecipitation (co-IP) was performed in UM-UC-3 cells via an anti-CTBS-GNG5 antibody or a negative control IgG antibody, followed by silver staining. The red arrows indicate the positions of the IGF2BP2 (upper band) and CTBS-GNG5 (lower band) protein signals. (B) Coimmunoprecipitation and western blotting analyses demonstrated the interaction between CTBS-GNG5 and IGF2BP2. (C) Representative immunofluorescence images illustrating the cytoplasmic colocalization of CTBS-

GNG5 and IGF2BP2 in UM-UC-3 cells. Nuclei are stained blue, IGF2BP2 is labelled green, and CTBS-GNG5 is shown in red. Scale bar (white) indicates 25 μm. (D) CTBS-GNG5 and IGF2BP2 protein levels in UM-UC-3 and A549 cells following *CTBS-GNG5* silencing or overexpression. (E) IGF2BP2 protein levels in various groups of UM-UC-3 cells following treatment with MG132 (10 μM) or DMSO for 12 h. (F) The total ubiquitination level of IGF2BP2 was assessed in *CTBS-GNG5*-knockdown UM-UC-3 and A549 cells transfected with the corresponding plasmids for 48 hours and subsequently treated with MG132 (10 μM) for 12 hours. (G) Total ubiquitination levels of IGF2BP2 were assessed in *CTBS-GNG5*-overexpressing UM-UC-3 and A549 cells transfected with the corresponding plasmids for 48 hours and subsequently treated with MG132 (10 μM) for 12 hours.

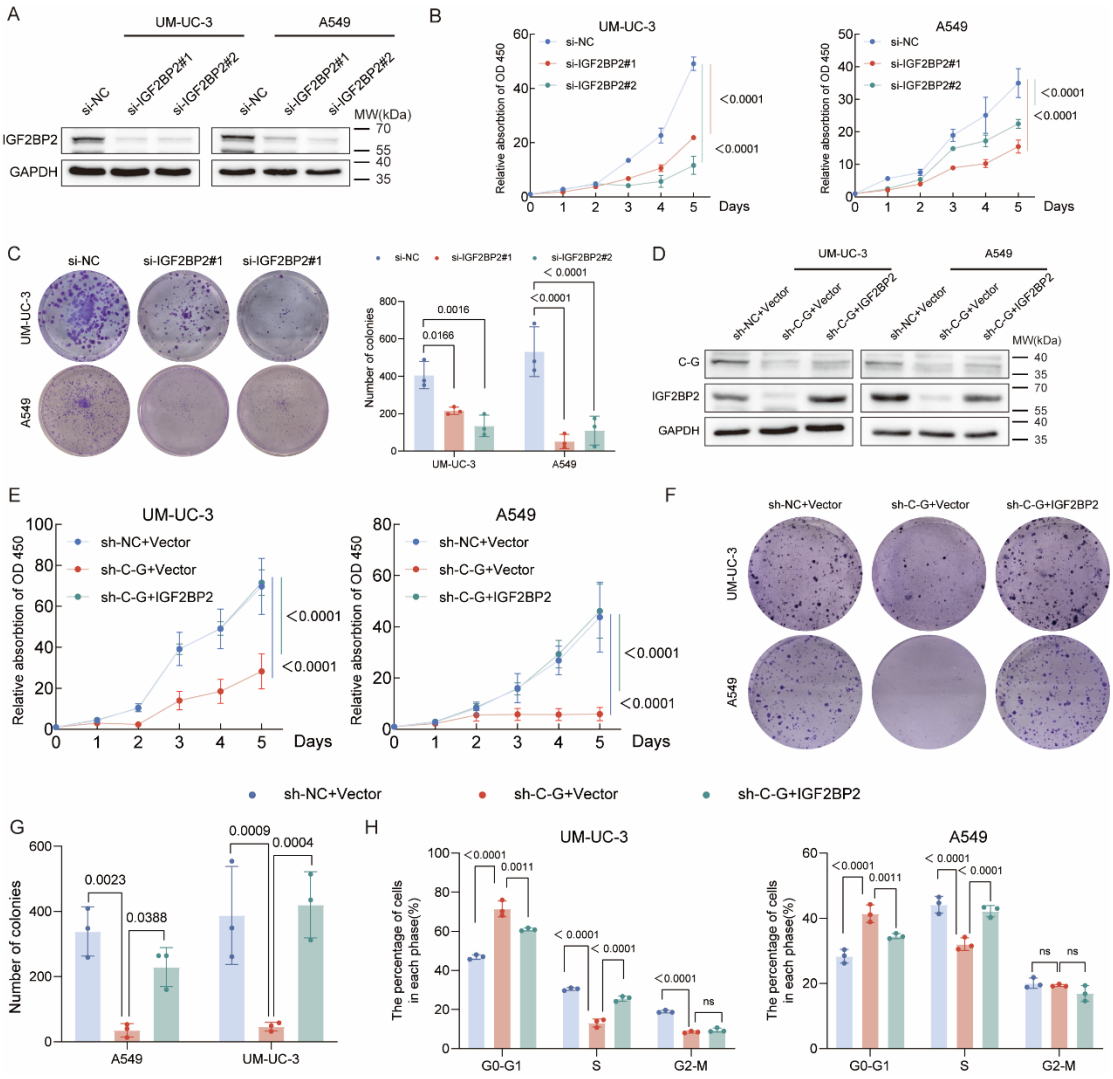

Figure 5. CTBS-GNG5 promotes cell proliferation by regulating IGF2BP2-mediated cell cycle progression.

(A) Western blot analysis of IGF2BP2 expression in the *IGF2BP2*-knockdown and control UM-UC-3 and A549 cell lines. (B) Cell viability was assessed via the CCK-8 assay in UM-UC-3 and A549 cell lines following *IGF2BP2* knockdown. (C) Representative images and quantitative histograms from colony formation assays are presented for UM-UC-3 and A549 cells after *IGF2BP2* knockdown. (D) Western blot analysis of CTBS-GNG5 and IGF2BP2 expression in *CTBS-GNG5*-knockdown or control UM-UC-3 and A549 cells overexpressing *IGF2BP2*. (E) Cell viability was assessed via the CCK-8 assay in UM-UC-3 and A549 cell lines following *CTBS-GNG5*-knockdown or control UM-UC-3 and A549 cells overexpressing *IGF2BP2*. (F-G) Representative images and quantitative histograms from colony formation assays are presented for UM-UC-3 and A549 cells after *CTBS-GNG5*-knockdown or control UM-UC-3 and A549 cells overexpressing *IGF2BP2*. (H) The percentages (%) of cell populations at different stages of the cell cycle are presented for *CTBS-GNG5*-knockdown or control UM-UC-3 and A549 cells overexpressing *IGF2BP2*. ns indicates not statistically significant. The data are expressed as the means ± SDs. Statistical significance was determined by one-way ANOVA with Tukey's post hoc test (C, G), and two-way ANOVA with Tukey's post hoc test (B, E, H).

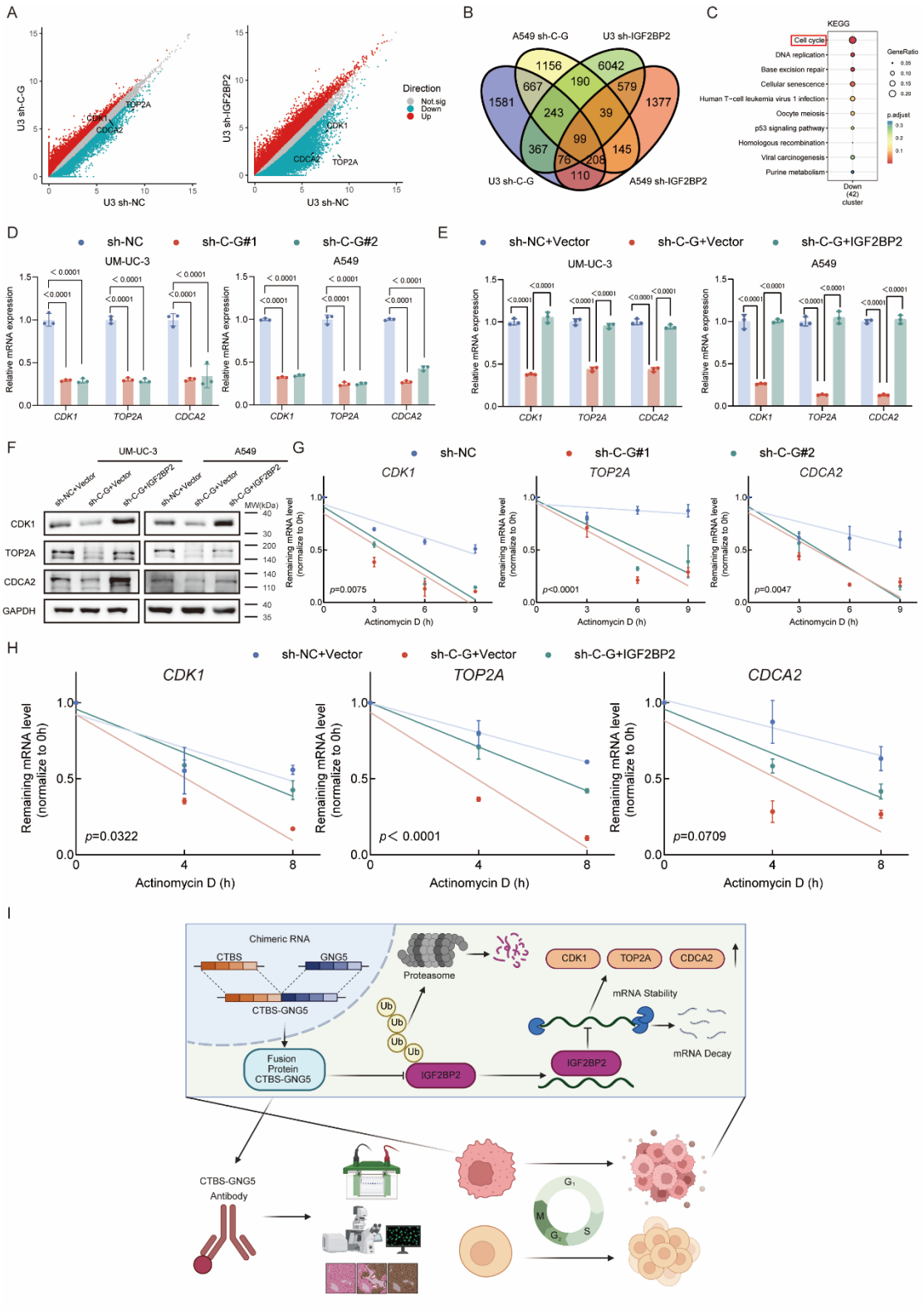

Figure 6. CTBS-GNG5 modulates the stability of *CDK1*, *TOP2A*, and *CDCA2* mRNAs in an IGF2BP2-dependent manner.

(A) Volcano plots illustrating the mRNA expression profiles of UM-UC-3 cells transfected with *CTBS-GNG5* or *IGF2BP2* siRNA. (B) A Venn diagram displaying the overlapping protein-coding genes downregulated in UM-UC-3 and A549 cells following the silencing of *CTBS-GNG5* or *IGF2BP2*. (C) Kyoto Encyclopedia of Genes and Genomes (KEGG) pathway analysis revealed enriched signalling pathways after *CTBS-GNG5* and *IGF2BP2* silencing. (D) qRT–PCR was conducted to evaluate the expression levels of CTBS-GNG5 target genes. (E–F) The mRNA and protein expression levels of CTBS-GNG5 target genes were assessed in *CTBS-GNG5*-knockdown cells and control cells overexpressing *IGF2BP2*. (G) A549 cells transfected with either control or sh-*CTBS-GNG5* constructs were treated with actinomycin D (5 mg/mL) for the specified time periods. (H) A549 cells with stable control expression, *CTBS-GNG5* knockdown, or *CTBS-GNG5* knockdown with *IGF2BP2* overexpression were treated with actinomycin D (5 mg/mL) for the indicated time periods. Total RNA was purified and analysed via qRT–PCR to determine the mRNA half-lives of *CDK1*, *TOP2A*, and *CDCA2*. (I) Proposed model showing that the CTBS-GNG5 fusion facilitates IGF2BP2-mediated regulation of the cell cycle in tissues and cells by modulating mRNA stability. The image was created via BioRender.com. The data are expressed as the means ± SDs. Statistical significance was determined by two-way ANOVA with Tukey's post hoc test (D, E), and Extra sum-of-squares F test (G, H).